


# Large magnon magnetoresistance of two-dimensional ferromagnets

Caleb Webb<sup>✉\*</sup> and Shufeng Zhang<sup>✉†</sup>

*Department of Physics, University of Arizona, Tucson, Arizona 85721, USA*

 (Received 2 April 2024; revised 2 August 2024; accepted 7 August 2024; published 3 September 2024)

The magnon current holds substantial importance in facilitating the transfer of angular momentum in spin-based electronics. However, the magnon current in three-dimensional magnetic materials remains orders of magnitude too small for applications. In contrast, magnon numbers in two-dimensional systems exhibit significant enhancement and are markedly influenced by external magnetic fields. Here, we investigate the magnon current in a two-dimensional easy-axis ferromagnet and find a large magnon magnetoresistance (LMMR) effect, wherein the change of the magnon conductance can reach as high as a thousand percent in a moderate magnetic field. Moreover, the magnitude of the LMMR exhibits significant dependence on the orientation of the magnetic field due to the interplay between magnon-conserving and non-magnon-conserving scattering. We propose a nonlocal magnon-mediated electrical drag experiment for the possible experimental observation of the predicted effect. With the LMMR effect and a much larger magnon number, magnon current in 2D materials shows promise as a primary source for spin transport in spintronics devices.

DOI: [10.1103/PhysRevB.110.104406](https://doi.org/10.1103/PhysRevB.110.104406)

## I. INTRODUCTION

Magnons, also known as spin wave quanta, are low-energy excitations of magnetically ordered states, holding significance in spintronics for their role in spin transport properties. Analogous to electron spins, magnons carry angular momenta and magnon current serves as a spin current that traverses magnetic media. Transport properties of magnons in various magnetically ordered states, including ferromagnetic, antiferromagnetic, and noncollinear magnetic structures, have been extensively investigated both experimentally and theoretically [1–9]. In these studies, the magnon current of three-dimensional magnets is generated through spin injection from boundaries or a thermal gradient; however, its magnitude remains orders of magnitude smaller than the conventional electron spin current, limiting the application of the magnon current as a primary source of spin information carriers.

Recent advances in the experimental development of two-dimensional (2D) magnetic materials [10–22] provide further opportunity to explore novel magnon transport. In particular, it has been demonstrated [5] that the magnon conductivity in thin YIG films greatly surpasses that of their three-dimensional counterparts. In this article we argue that magnon transport should see an even greater enhancement in a truly two-dimensional ferromagnetic insulator. Compared to conventional magnon transport properties in 3D systems, low-dimensional magnets experience much stronger spin fluctuations. Owing to the Mermin-Wagner theorem, thermal fluctuations destroy long-range magnetic ordering for the isotropic short-range Heisenberg Hamiltonian [23] and the spatial random field breaks the uniform magnetization into domains [24]. Breaking the continuous  $SO(3)$  symmetry by

introducing magnetocrystalline anisotropy and/or external field induces a gap,  $\Delta$ , in the excitation spectrum. In the long-wavelength limit, the magnon dispersion is given by  $\omega_k \sim \Delta + Jk^2$ , where  $J$  is the exchange constant. The equilibrium magnon number  $N_0 = \int d^2k [\exp(\beta\omega_k) - 1]^{-1}$  (with inverse temperature  $\beta$ ) varies weakly with the gap but diverges logarithmically as  $\Delta \rightarrow 0$ . If there is any magnetic anisotropy in the sample the magnon number remains finite, but still much larger than that for a three-dimensional magnet. Since the gap can be controlled by the external magnetic field, one would expect that the magnon number varies strongly with external field. The magnon conductivity,  $\sigma \sim N_0\tau$ , with  $\tau$  the magnon lifetime, is therefore expected to be much more sensitive to an external magnetic field in a two-dimensional sample, implying a larger magnon magnetoresistance (MMR) effect is possible.

In this article we demonstrate that the influence of the external field on the magnon lifetime and gap leads to a large magnon magnetoresistance (LMMR) in two-dimensional ferromagnets with easy-axis exchange anisotropy. We find that for fields parallel to the easy axis the magnon transport properties are governed primarily by changes in equilibrium magnon number. However, nonparallel fields generate non-magnon-conserving scattering processes [25] which greatly reduce the lifetime at small field strengths in 2D. By explicitly calculating the magnon conductance for this model, we find the magnetoresistance could reach thousands of percent for a moderate strength of the magnetic field. Furthermore, MMR is highly dependent on the direction of the field due to the competition between the magnon-conserving and non-magnon-conserving scattering in the model Hamiltonian. Such large magnon magnetoresistance is orders of magnitude larger than the conventional magnetoresistance of magnetic materials and is comparable to the magnetic oxides near the metal-insulator transition temperatures [26–29]. We emphasize, however, that the MMR presented in this article does

\*Contact author: [calebmwebb@arizona.edu](mailto:calebmwebb@arizona.edu)

†Contact author: [zhangshu@arizona.edu](mailto:zhangshu@arizona.edu)

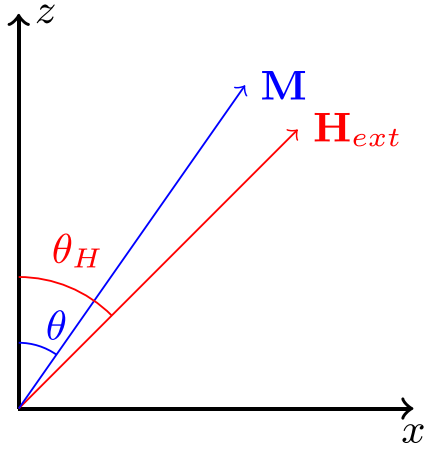


FIG. 1. Equilibrium magnetization direction  $\mathbf{M}$  in the presence of an external field  $\mathbf{H}_{\text{ext}}$  in the  $xz$  plane.

not rely on any phase transition, and the underlying physical mechanism is entirely different from that of the colossal magnetoresistance in magnetic perovskite materials.

The remainder of this article is organized as follows. In Sec. II we introduce the model Hamiltonian and derive the scattering vertices. In Sec. III the scattering widths are discussed. The magnon magnetoresistance effect is presented in Sec. IV, and a possible experimental realization is discussed in Sec. V.

Throughout this article we set  $\hbar = k_B = c = 1$ .

## II. MODEL

We consider an easy-axis ferromagnetic Heisenberg model on a two-dimensional lattice with out-of-plane exchange anisotropy and arbitrary external field  $\mathbf{H}_{\text{ext}}$ , which points at an angle  $\theta_H$  from the  $z$  axis. The Hamiltonian is

$$H = -\sum_{(i,j)} (J\mathbf{S}_i \cdot \mathbf{S}_j + J_z S_i^z S_j^z) - \sum_i \mathbf{H}_0 \cdot \mathbf{S}_i, \quad (1)$$

with  $J > 0$  the isotropic exchange coupling and  $J_z > 0$  the exchange anisotropy, taken along the positive  $z$  axis.  $\mathbf{S}_i$  is the spin operator for lattice site  $i$ , and in the first term we sum over nearest neighbors  $i$  and  $j$ . The parameter  $\mathbf{H}_0 = \mu \mathbf{H}_{\text{ext}}$ , with  $\mu$  the magnetic moment per unit spin, has been introduced as shorthand. Competition between the anisotropy and external field will shift the ground state magnetization away from the easy axis ( $z$  axis). We describe the equilibrium magnetization  $\mathbf{M}$  by an angle  $\theta$  as in Fig. 1. In order to expand Eq. (1) about its classical ground state, the spin operators are first expressed in a rotated frame,  $\mathbf{S} = \mathbf{R}\mathbf{S}'$ , with the  $z'$  axis parallel to  $\mathbf{M}$ . In this rotated frame Eq. (1) becomes

$$\begin{aligned} H = & -\sum_{(i,j)} (J\mathbf{S}'_i \cdot \mathbf{S}'_j + J_z [\sin^2 \theta S_i^x S_j^x + \cos^2 \theta S_i^z S_j^z \\ & - \sin \theta \cos \theta (S_i^x S_j^z + S_i^z S_j^x)]) \\ & - \sum_i (H_0^x [\cos \theta S_i^x + \sin \theta S_i^z] \\ & + H_0^z [-\sin \theta S_i^x + \cos \theta S_i^z]), \end{aligned} \quad (2)$$

which may now be expanded in small fluctuations by means of the usual Holstein-Primakoff (HP) transformation. Up to cubic order in the boson operators we have

$$\begin{aligned} S_i^z &= S - a_i^\dagger a_i, & S_i^+ &= \sqrt{2S} \left( 1 - \frac{a_i^\dagger a_i}{4S} \right) a_i, \\ S_i^- &= \sqrt{2S} a_i^\dagger \left( 1 - \frac{a_i^\dagger a_i}{4S} \right). \end{aligned} \quad (3)$$

This truncation of the HP transformation is sufficient to produce the lowest order corrections to the magnon lifetime at low temperatures ( $T \ll T_C$  with  $T_C$  the Curie temperature), where the magnon density is not too large. Applying Eq. (3) to Eq. (2) yields the Hamiltonian for the interacting magnon system,  $H = H^{(0)} + H^{(1)} + H^{(2)} + H^{(3)} + H^{(4)}$  with  $H^{(n)}$  containing  $n$  boson operators. The first two terms are

$$H^{(0)} = -SN[\alpha + \alpha_z \cos^2 \theta + H_0 \cos(\theta_H - \theta)], \quad (4)$$

$$H^{(1)} = \sqrt{\frac{S}{2}} [\alpha_z \sin 2\theta - H_0 \sin(\theta_H - \theta)] \sum_i a_i^\dagger + a_i, \quad (5)$$

and describe the classical ground state energy and shift due to uniform canting of the lattice spins toward the anisotropy axis, respectively. Above, we have defined the anisotropy and exchange parameters  $\alpha_z = J_z SN_\delta$  and  $\alpha = JSN_\delta$ , with  $N_\delta$  the number of nearest neighbors for each lattice site.  $N$  is the total number of lattice sites. For simplicity, we assume a lattice with inversion symmetry. The angle  $\theta$  is defined by minimizing  $H^{(0)}$ , or equivalently, setting  $H^{(1)} = 0$ , and is given by the solution to

$$\alpha_z \sin(2\theta) = H_0 \sin(\theta_H - \theta). \quad (6)$$

The interacting magnon Hamiltonian is then obtained by application of the Fourier transform  $a_i = \frac{1}{\sqrt{N}} \sum_k e^{i\mathbf{k} \cdot \mathbf{R}_i} a_k$ :

$$\begin{aligned} H = & \sum_k \omega_k a_k^\dagger a_k + V_k^{(2)} (a_k a_{-k} + a_{-k}^\dagger a_k^\dagger) \\ & + \frac{1}{\sqrt{N}} \sum_{k_1, k_2, k_3} V_{k_1, k_2, k_3}^{(3)} (a_{k_1}^\dagger a_{k_2}^\dagger a_{k_3} + a_{k_3}^\dagger a_{k_2} a_{k_1}) \\ & + \frac{1}{N} \sum_{k_1, k_2, k_3, k_4} V_{k_1, k_2, k_3, k_4}^{(4)} a_{k_1}^\dagger a_{k_2}^\dagger a_{k_3} a_{k_4}. \end{aligned} \quad (7)$$

Defining the lattice factor  $\gamma_k = \frac{1}{N_\delta} \sum_\delta e^{-\mathbf{k} \cdot \delta}$ , with  $\delta$  a vector from each site to its nearest neighbors, the full magnon dispersion and interaction vertices are

$$\begin{aligned} \omega_k = & -(2\alpha + \alpha_z \sin^2 \theta) \gamma_k + 2(\alpha + \alpha_z \cos^2 \theta) \\ & + H_0 \cos(\theta_H - \theta), \end{aligned} \quad (8)$$

$$V_k^{(2)} = -\frac{\alpha_z \sin^2(\theta)}{2} \gamma_k, \quad (9)$$

$$V_{k_1, k_2, k_3}^{(3)} = -\frac{\delta_{k_1+k_2-k_3}}{\sqrt{2S}} \alpha_z \sin(2\theta) \gamma_{k_1}, \quad (10)$$

$$V_{k_1, k_2, k_3, k_4}^{(4)} = \frac{\delta_{k_1+k_2-k_3-k_4}}{2S} \alpha (\gamma_{k_4} + \gamma_{k_1} - 2\gamma_{k_2-k_3}). \quad (11)$$

Since we have limited our analysis to the lowest order corrections to the magnon lifetime, it is sufficient to consider only terms up to order  $O(a^4)$ . Moreover, the off-diagonal terms  $V_k^{(2)}(a_k a_{-k} + a_k^\dagger a_{-k}^\dagger)$  are treated as scattering processes in the Dyson series for the self-energy. To lowest order in  $\alpha_z$  they do not contribute any broadening and are from here on neglected. Our treatment is similar to that in [30] in the limit  $T \gg \alpha_z$ . Additionally, in  $H^{(4)}$  we have neglected terms proportional to  $\alpha_z$  on the grounds that  $J_z \ll J$ , and so the two-magnon scattering processes will be dominated by the exchange coupling.

For a square lattice in the long-wavelength limit the magnon frequency reduces to the quadratic form  $\omega_k = \Delta + \omega_0 k^2$  with gap

$$\Delta = \alpha_z(3 \cos^2 \theta - 1) + H_0 \cos(\theta_H - \theta) \quad (12)$$

and frequency

$$\omega_0 = \frac{2\alpha + \alpha_z \sin^2 \theta}{4} \approx \alpha/2. \quad (13)$$

The frequency is governed primarily by the exchange coupling, and is largely unaffected by the external field. The gap, Eq. (12), is strongly dependent on the field strength and has a somewhat complicated relationship with the field direction. Numerically analysis of Eqs. (12) and (6) shows that  $\Delta$  develops a minimum for  $H_0 > 0$  when  $\theta_H \geq \theta_c \approx 0.424\pi$ . This minimum reaches its lowest value of  $\Delta_{\min} = \alpha_z$  when  $\theta_H = \pi/2$  and at the critical field  $H_c = 2\alpha_z$ . For  $\theta_H < \theta_c$  the gap is a monotonically increasing function of the external field.

In this limit the interaction vertices reduce to

$$V_{k_1, k_2, k_3}^{(3)} = -\frac{\delta_{k_1+k_2-k_3}}{\sqrt{2S}} \alpha_z \sin(2\theta)(1 - k_1^2/4), \quad (14)$$

$$V_{k_1, k_2, k_3, k_4}^{(4)} = \frac{\delta_{k_1+k_2-k_3-k_4}}{8S} \alpha [k_4^2 + k_1^2 - 2(k_2 - k_3)^2]. \quad (15)$$

The potential  $V^{(3)}$  in Eq. (7) describes the spontaneous decay of one magnon into two, and vice versa, and is strongly dependent on the direction of the external field. From Eq. (6) one finds that for  $\theta_H = 0, \theta = 0$  and for field strengths  $H_0 > 2\alpha_z$ ,  $\theta_H = \pi/2 \Rightarrow \theta = \pi/2$ . We conclude that non-magnon-conserving processes ( $V^{(3)}$ ) vanish for external fields parallel to the easy axis, or for fields  $H_0 > H_c = 2\alpha_z$  perpendicular to it. The final term in Eq. (7) describes magnon-magnon scattering with potential  $V^{(4)}$  which is independent of the equilibrium magnetization direction [see Eq. (15)]. Importantly, this potential is directly proportional to the magnon energy,  $V^{(4)} \sim Jk^2$ , which is assumed small. For thermal magnons  $Jk^2 \sim T$ , and these two vertices may be comparable over a wide range of magnon energy for temperature well below  $T_C$ .

### III. SCATTERING WIDTHS

The scattering widths for each process are calculated to single-loop order using the standard diagrammatic techniques [31,32]. We denote by  $\Gamma_{NC}$  the width for non-magnon-conserving scattering ( $V^{(3)}$ ), and by  $\Gamma_C$  for magnon-conserving scattering ( $V^{(4)}$ ). These scattering widths are plotted as a function of the dimensionless energy parameter  $z = \omega_0 k^2/T$  for several different external field magnitudes in

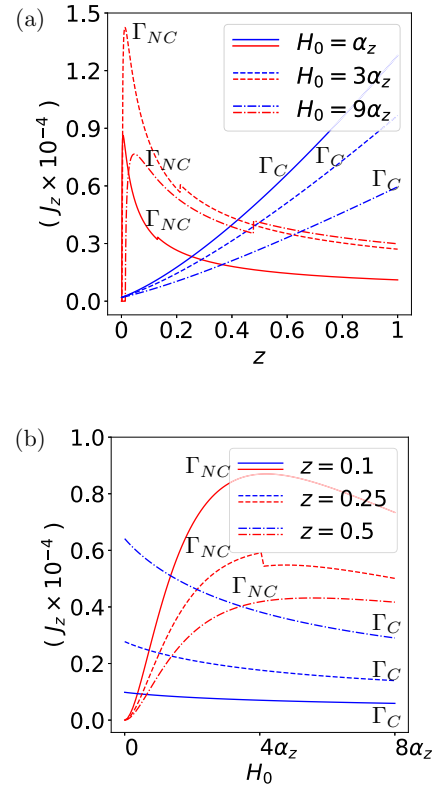


FIG. 2. Comparison of the non-magnon conserving and magnon conserving scattering widths for external field at an angle  $\theta_H = \pi/6$  to the easy-axis. (a) Scattering widths as a function of the dimensionless energy parameter  $z = \omega_0 k^2/T$  for different external field strengths  $H_0$ . (b) Widths as a function of external field strength for different  $z$  in the range  $0 < z < 1$ . We use red curves for  $\Gamma_{NC}$  and blue for  $\Gamma_C$ . The parameters chosen here are  $J_z/J = 10^{-5}$  and  $T/T_C = 10^{-2}$ . We assume a square lattice in the long-wavelength limit, for which the Curie temperature is approximately  $T_C/J \sim 0.1$ . The momentum cutoff  $z_c$  is chosen so that  $\omega_k \lesssim T$ .

Fig. 2. The results presented above are for the field angle  $\theta_H = \pi/6$ , but remain qualitatively similar for  $0 < \theta_H < \theta_c$ . For parallel fields,  $\Gamma_{NC} = 0$  but otherwise the results for  $\Gamma_C$  are mostly unaffected. Fields at angles  $\theta_H \geq \theta_c$  have a more significant influence on  $\Gamma_{NC}$ , and this case is discussed separately below. Full details of these calculations can be found in the Appendix. Here, we briefly summarize some of the more salient features found within Fig. 2.

The peak in  $\Gamma_{NC}$  in Fig. 2(a) can be understood as follows. The vertex  $V^{(3)}$  for nonconservative scattering is independent of momentum, and so apart from an energy-conserving cutoff at very low magnon energy (see Appendix), this scattering width is governed by the Bose distribution and therefore dominated by low-energy magnons. Above the cutoff, then,  $\Gamma_{NC}$  rises sharply to its peak before quickly decaying toward higher energies. Because the magnon-conserving vertex  $V^{(4)}$  scales with momentum,  $\Gamma_C$  is suppressed at low energies.

From Fig. 2(a) it is apparent that the width  $\Gamma_C$  is suppressed by an increasing external field, consistent with the notion that increasing the gap suppresses the number of magnons, thereby reducing the scattering width. The relationship between  $\Gamma_{NC}$  and  $H_0$  is, however, more complex. This is shown more clearly

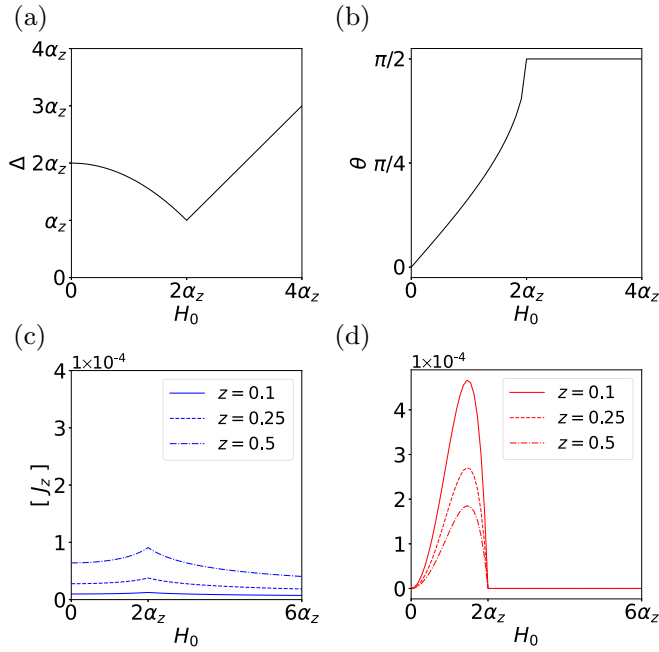


FIG. 3. (a) Energy gap, (b) equilibrium magnetization direction, (c) magnon-conserving scattering width, and (d) non-magnon-conserving scattering width as a function of external field strength for in-plane fields. All other parameters are as in Fig. 2.

in Fig. 2(b), in which we plot each scattering width as a function of external field strength at several values of  $z$  within the available momentum range. The peak in  $\Gamma_{NC}$  results from competition between the strengthening vertex [Eq. (14)] and widening gap. As  $H_0$  increases, the magnetization angle  $\theta$  increases from zero and approaches the limit  $\theta_H$ . At the same time, the gap [Eq. (12)] increases monotonically for  $\theta_H < \theta_c$ . The width  $\Gamma_{NC}$ , then, increases from zero until the magnetization angle is saturated by the external field, at which point the increase in vertex strength is overtaken by the growth in  $\Delta$ .

For field angles  $\theta_H \geq \theta_c$  the gap does not increase monotonically with field, but develops a minimum for small  $H_0$ . This is most pronounced for in-plane fields, where the minimum is reached exactly as the magnetization is saturated by the external field,  $\theta \rightarrow \pi/2$ . Both scattering widths should therefore be *increasing* for  $0 \leq H_0 < 2\alpha_z$ . The vertex  $V^{(3)}$ , however, vanishes when the magnetization switches to in-plane, and so  $\Gamma_{NC}$  drops abruptly to zero from its maximum value at the critical field  $H_c$ . The full scattering width, then, will change dramatically as the field is tuned across this critical point (see Fig. 3).

#### IV. MAGNON MAGNETORESISTANCE

The magnon conductivity can be calculated from a linearized Boltzmann equation in the relaxation time approximation  $\sigma = \int d^2 p v^2 \partial n / \partial \omega \tau$ , or,

$$\sigma = \frac{4\pi}{\beta} \int_0^{z_c} dz \frac{z e^{z+\beta\Delta}}{\Gamma(z)(e^{z+\beta\Delta} - 1)^2}, \quad (16)$$

where  $\Gamma = \Gamma_{NC} + \Gamma_C$ . From Figs. 2 and 3 it is clear that the nonconservative scattering is dominant in the small-

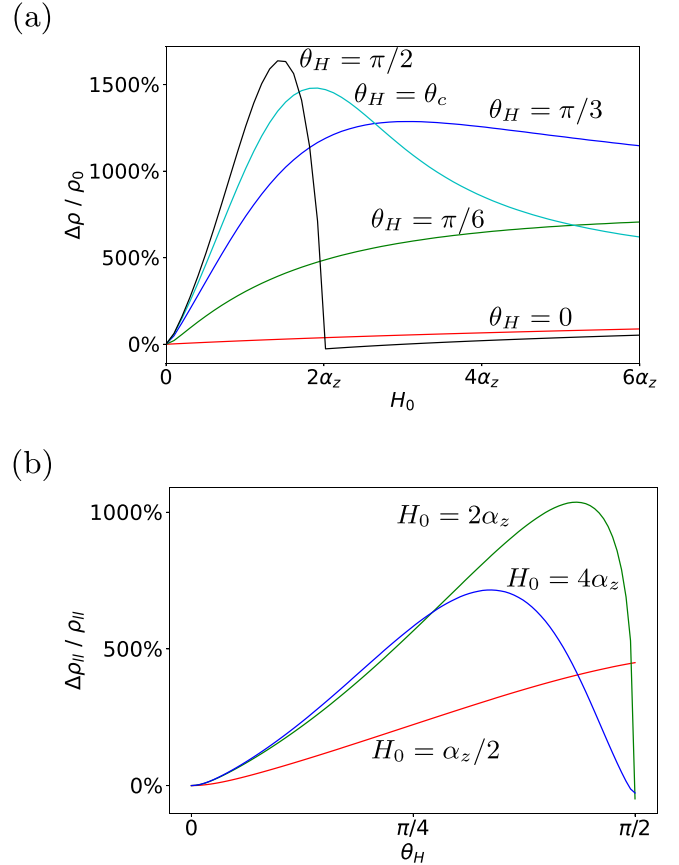


FIG. 4. LMMR effect as a function of external field strength and direction. (a) Magnon magnetoresistance ratio at several different directions of the external field. (b) Anisotropic magnon magnetoresistance ratio at several different strengths of the field.

momentum regime, where the Bose distribution is largest. One therefore anticipates that these processes have a greater influence over the conductivity. Indeed, we find a large MMR effect for nonparallel external fields. Of particular interest are in-plane fields, for which we find a significant spike in the magnon resistivity at fields  $H_0 < 2\alpha_z$  which drops rapidly to zero at the critical point. In Fig. 4(a) we present the magnon magnetoresistance ratio as a function of external field strength. In the figure  $\rho_0 = \rho(H_0 = 0)$  and  $\Delta\rho = \rho - \rho_0$ . The magnon conductivity is also influenced by the direction of the external field, and the anisotropic magnon magnetoresistance ratio is plotted in Fig. 4(b). Here  $\rho_{\parallel} = \rho(\theta_H = 0)$  and  $\Delta\rho_{\parallel} = \rho - \rho_{\parallel}$ . That this LMMR should be so large can, again, be seen as a consequence of the sharply peaked width  $\Gamma$  due to nonconservative scattering. Heuristically,  $\rho \sim \langle \Gamma \rangle / N_0$  with  $\langle \cdot \rangle$  denoting the thermal average over the Bose distribution. Due to its logarithmic dependence on the gap,  $N_0$  is only slightly influenced by the external field compared to  $\Gamma$  for nonparallel fields. The MMR is then governed primarily by the nonconservative scattering processes at low temperatures.

It should be noted that the predicted LMMR is most pronounced for field strengths  $H_0 \sim \alpha_z$ , and is significantly less pronounced for larger fields. The anisotropic MMR, however, remains significant for  $H > H_c$  [see Fig. 4(b)]. At the critical field, the magnon resistivity is enhanced by as much as 1000%

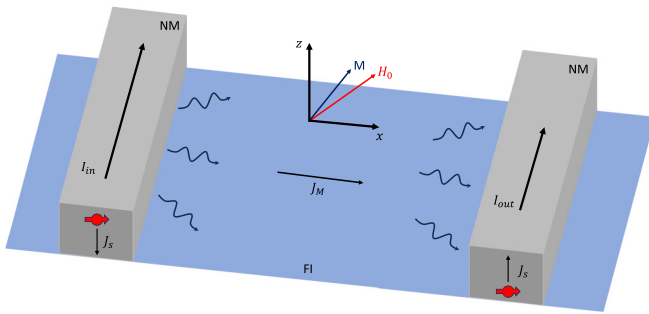


FIG. 5. Schematic of experimental setup for nonlocal electrical drag measurement. Two metallic strips (NM) are placed some distance apart on a two-dimensional ferromagnetic insulator (FI). Driving a current ( $I_{in}$ ) in the left strip injects a spin current ( $J_s$ ) into the FI via the spin Hall effect. This in turn excites a magnon current ( $J_M$ ) which is transported diffusively through the FI where it encounters the other NM strip. Here, the magnon current excites a spin current which is then converted to an electrical current  $I_{out}$  via the inverse spin Hall effect.

relative to its value at parallel field. However, even at much larger fields the MMR can reach up to 500%.

## V. EXPERIMENTAL REALIZATION

We now elaborate on potential experimental approaches to realize the predicted LMMR effect. Typically, the magnon current is investigated either by the spin Seebeck effect [1] through inducing a temperature gradient or by applying an electric current in a heavy metal, thus injecting a spin Hall current into the contacting magnetic layer [4,5]. Here, we focus on the latter method, wherein the magnetic layer is a 2D magnet insulator. The setup proposed here differs from the magnon conductivity measurements in thin YIG films of [5] only in that the magnetic layer is two-dimensional, and the external field is allowed out of the sample plane.

As in Fig. 5 the injected spin current excites a magnon current in the magnetic layer which is then converted into a spin current in another metal layer some distance away. The spin current is then converted to an electrical current via the inverse spin Hall effect. The resistance of the device can be readily determined from the nonlocal voltage produced, from which the magnon conductivity can be deduced.

Given that the spin direction of the spin Hall current from the heavy metal is in-plane, the magnon current would predominantly respond to the in-plane component of the magnetization. By manipulating the magnitude and orientation of the applied magnetic field, one can align the magnetization in any desired direction, accommodating either perpendicular or in-plane anisotropy of the 2D magnet. Assuming magnon scattering dominates over other forms of scattering such as magnetic defects, the observed inverse spin Hall signals in the detecting heavy metal bar would delineate the magnitude and directional dependence of the magnetic field, effectively manifesting the predicted LMMR effect.

## VI. DISCUSSION

In conclusion, we have calculated the magnon conductance of the ferromagnetic Heisenberg model on a two-dimensional

lattice with out-of-plane exchange anisotropy and external magnetic fields. Due to the inherently strong spin fluctuations in this low-dimensional system, the magnon population and conductance are much larger compared to those in three-dimensional systems. More interestingly, the external magnetic field has a profound effect on the magnon conductance, leading to significant magnon magnetoresistance (LMMR). Furthermore, we find that the LMMR is highly dependent on the orientation of the external field, primarily due to non-magnon-conserved scattering processes where the significant angular dependence of magnon scattering plays a dominant role in LMMR. These properties provide an encouraging prospect for the application of 2D magnets in spintronic devices, where the magnon current serves as angular momentum carriers.

Both magnon-conserving and non-magnon-conserving scattering are present in three dimensions as well, suggesting that an anisotropic magnetoresistance effect is not unique to low-dimensional systems. We have argued, however, that the effect is amplified in two dimensions. The ratio of non-magnon-conserving scattering widths in two dimensions to that of three dimensions can be shown to scale as [see discussion at the end of Appendix 1 and Eq. (A9)]

$$\frac{\Gamma_{NC}^{(2D)}}{\Gamma_{NC}^{(3D)}} \sim \left[ \sqrt{\frac{\Delta}{\omega_0}} \ln \frac{1}{\beta\Delta} \right]^{-1}. \quad (17)$$

Clearly, this ratio diverges in the limit  $\Delta \rightarrow 0$ , signaling that the anisotropic magnetoresistance effect should be enhanced by the stronger fluctuations in two-dimensional systems.

We wish to point out that two other magnon scattering mechanisms may reduce the LMMR. The magnon-phonon interactions are always present in 2D magnetic insulators. Further study is needed to quantitatively determine the relative strength of magnon-phonon contributions in order to determine the conditions under which the LMMR effect is observable in a realistic sample. Additionally, magnetic impurities, defects, and interface roughness could also be significant sources of scattering. However, we expect that such scattering will be limited with the improvement of high-quality 2D single crystals.

## ACKNOWLEDGMENT

This work is supported by National Science Foundation (NSF) Grant No. ECCS-2401267.

## APPENDIX: DERIVATION OF SCATTERING WIDTHS

In this section we derive in detail the two scattering widths,  $\Gamma_{NC}$  and  $\Gamma_C$ , from the usual Matsubara formalism in Green's function theory.

### 1. Nonconservative scattering

Up to one-loop order in the Dyson series, the second line in Eq. (7) generates the two self-energy diagrams shown in Fig. 6. The polarization-bubble type diagram,  $\Sigma_{3a}$ , is a finite-temperature effect which dominates the magnon lifetime for  $T > 0$ .  $\Sigma_{3b}$ , on the other hand, describes spontaneous magnon decay and is present even at  $T = 0$  [33,34].

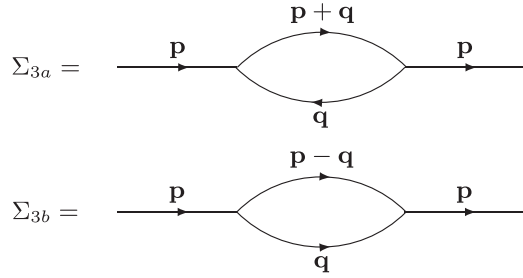


FIG. 6. All single-loop order corrections to the self-energy generated by the cubic terms in Eq. (7). Vertices are given by Eq. (14).

Following the Matsubara formalism these corrections are calculated as, respectively,

$$\Sigma_{3a}(\omega, \mathbf{k}) = \frac{1}{N} \sum_q [V_q^{(3)} + V_k^{(3)}]^2 \frac{n(\omega_{k+q}) + n(\omega_q)}{i\omega - \omega_{k+q} + \omega_q}, \quad (\text{A1})$$

$$\Sigma_{3b}(\omega, \mathbf{k}) = \frac{1}{N} \sum_q V_{k-q}^{(3)} [V_{k-q}^{(3)} + V_q^{(3)}] \frac{1 + n(\omega_q) - n(\omega_{k-q})}{i\omega - \omega_q - \omega_{k-q}}. \quad (\text{A2})$$

Above,  $n(\omega) = (e^{\beta\omega} - 1)^{-1}$  is the equilibrium magnon distribution at inverse temperature  $\beta = 1/T$ , and all sums over constrained momenta have been carried out so that the vertices read  $V_k^{(3)} = V_0(1 - \frac{1}{6}k^2)$  in the long-wavelength limit, where  $V_0 = \frac{\alpha_z}{\sqrt{23}} \sin(2\theta)$ . Within this limit integration is commonly carried out over all  $\mathbf{q} \in \mathbb{R}^2$ , reasoning that any error introduced by including large  $q$  should be suppressed by the Bose distributions. However, these processes involve spontaneous creation/annihilation of magnons. Due to the presence of the gap,  $\omega_k = \Delta + \omega_0 k^2$ , the initial and final states must have a finite energy, and so there must be a lower bound for the external momenta in Fig. 6. As will be shown below, this lower bound is sensitive to the choice of integration cutoff for the internal momentum,  $q_c$ .

The scattering widths for Eqs. (A1) and (A2) are constrained on-shell by the following kinematic relations.  $\Gamma_{3a}(\mathbf{k}) = -2\text{Im}(\Sigma_{3a}) > 0$  only for momenta  $\mathbf{k}$  satisfying  $\omega_k = \omega_{k+q} - \omega_q \Rightarrow 2\omega_0 \mathbf{k} \cdot \mathbf{q} = \Delta$ . For finite internal momentum  $q$ , then, the available scattering states are bounded below by  $k > \Delta/2\omega_0 q_c$ .  $\Gamma_{3b}$  is constrained by  $\omega_k = \omega_{k-q} + \omega_q$ , which is satisfied only for  $q \in [q_-, q_+]$  with

$$q_{\pm} = \frac{1}{2}(k \pm \sqrt{k^2 - 2\Delta/\omega_0}). \quad (\text{A3})$$

These decay processes are therefore only allowed for magnons with a kinetic energy  $\omega_0 k^2 > 2\Delta$ , which is a sensible

constraint for the spontaneous emission of two magnons with a gapped spectrum.

The momentum cutoff is chosen so that  $\omega_k \lesssim T$ , and so the Bose distributions can be roughly approximated as  $n(\omega) \sim 1/\beta\omega$ . Then

$$\Gamma_{3a} \approx \frac{2V_0^2}{\pi\beta} \int d^2\mathbf{q} \left( \frac{1}{\omega_q} + \frac{1}{\omega_p + \omega_q} \right) \delta(2\omega_0 p q \cos\phi - \Delta), \quad (\text{A4})$$

where we have ignored the momentum dependence of the vertex. The  $\delta$  function is used to eliminate the integral over angle, yielding

$$\Gamma_{3a} = \frac{2V_0^2 q_0}{\pi\beta\Delta} \int_{q_0}^{q_c} \frac{q dq}{\sqrt{q^2 - q_0^2}} \left( \frac{1}{\omega_q} + \frac{1}{\omega_q + \omega_p} \right) \quad (\text{A5})$$

with  $q_0(k) = \Delta/2\omega_0 k$ . As  $k \rightarrow \frac{\Delta}{2\omega_0 q_c}$ ,  $\Gamma_{3a} \rightarrow 0$ . Similarly,

$$\Gamma_{3b} = \frac{V_0^2}{\pi\beta} \int_{q_-}^{q_+} \frac{q dq}{\sqrt{(q_+^2 - q^2)(q^2 - q_-^2)}} \times \left( 1 + \frac{1}{\omega_q} - \frac{1}{\omega_k - \omega_q} \right). \quad (\text{A6})$$

Both integrations are easily carried out. In terms of the dimensionless variables  $z = \beta\omega_0 k^2$ ,  $z_c = \beta\omega_0 q_c^2$ , and  $z_- = \beta\omega_0 q_-^2$ ,

$$\Gamma_{3a} = \frac{V_0^2}{\pi\omega_0} \left[ \frac{\tan^{-1} \left( \sqrt{\frac{4z_c(z-z_-)}{\beta\Delta(4z+\beta\Delta)}} \right)}{\sqrt{\beta\Delta(4z+\beta\Delta)}} + \frac{\tan^{-1} \left( \sqrt{\frac{4z_c(z-z_-)}{(2z+\beta\Delta)^2 + 4z\beta\Delta}} \right)}{\sqrt{(2z+\beta\Delta)^2 + 4z\beta\Delta}} \right]. \quad (\text{A7})$$

To leading order in  $\beta\Delta$  this width scales as  $\Gamma_{3a} \sim V_0^2/4\omega_0\sqrt{z\beta\Delta}$ . The enhancement with decreasing gap can be understood as a consequence of the increase in magnon number. As  $\Delta$  decreases, there are more magnons in the system, and therefore more scattering events.

For the spontaneous decay we obtain

$$\Gamma_{3b} = \frac{V_0^2}{8\omega_0} \Theta(z - 2\beta\Delta). \quad (\text{A8})$$

Apart from the constraint  $z > 2\beta\Delta$  this width is independent of momentum, temperature, and gap. For small fields  $\Gamma_{3a} \gg \Gamma_{3b}$  and so this spontaneous decay process has only a small

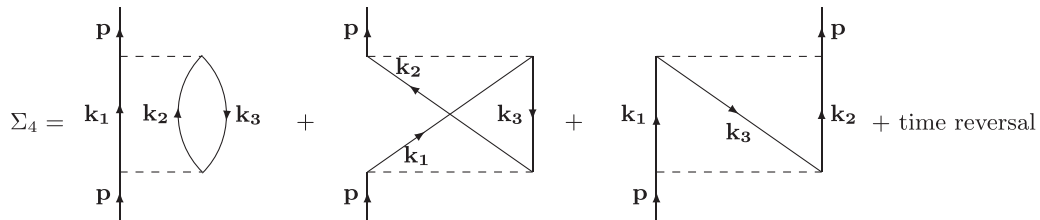


FIG. 7. All single-loop order corrections to the self-energy generated by the quartic terms in Eq. (7). Following [32], the dashed lines represent vertices given by Eq. (15) and solid lines are magnon lines. We include among these corrections the time reversal of each diagram, in order to account for detailed balance [35,36].

influence on the magnon lifetime above zero temperature. The discontinuity at  $z = 2\beta\Delta$  is responsible for the sudden jumps in  $\Gamma_{NC}$  in Fig. 2.

The enhancement of the scattering is not strictly unique to two-dimensional systems, though it is straightforward to show that the scaling for this width with  $\Delta$  in three dimensions is weaker. Beginning from Eq. (A4) and adjusting the integral for three-dimensional scattering it is found that  $\Gamma_{3a}^{3D} \sim V_0^2 \ln(1/\beta\Delta)/(4\pi^2 \sqrt{z\beta\omega_0^3})$ . Similarly,  $\Gamma_{3b}^{3D} \sim V_0^2/4\pi^2 \sqrt{(z-2\beta\Delta)/4\beta\omega_0}$ . As in the two-dimensional case, this term does not contribute significantly to the overall scattering width. The ratio of the non-magnon-conserving widths in two dimensions to three therefore scales as

$$\frac{\Gamma_{NC}^{2D}}{\Gamma_{NC}^{3D}} \sim \left[ \sqrt{\frac{\Delta}{\omega_0}} \ln\left(\frac{1}{\beta\Delta}\right) \right]^{-1}. \quad (\text{A9})$$

Clearly the ratio diverges as  $\Delta \rightarrow 0$ , suggesting that  $\Gamma_{NC}$ , and therefore the anisotropic magnetoresistance effect, is enhanced by the larger spin fluctuations in two-dimensional systems.

## 2. Conservative scattering

Following the general procedure for calculating self-energy corrections due to two-particle scattering outlined in [32], we consider the following first-order self-energy diagrams (Fig. 7), generated by the quartic terms in Eq. (7).

Excluding the time-reversed contributions, the self-energy correction is

$$\begin{aligned} \Sigma_4 &= \frac{1}{N^2} \sum_{k_1, k_2, k_3} V_{1,2,p,3}^{(4)} (2V_{p,3,1,2}^{(4)} + V_{p,3,2,1}^{(4)}) \\ &\times \frac{[1 + n(\omega_{k_1})][1 + n(\omega_{k_2})]n(\omega_{k_3})}{i\omega - \omega_{k_1} - \omega_{k_2} + \omega_{k_3}}. \end{aligned} \quad (\text{A10})$$

The time-reversed diagrams are a consequence of detailed balance, and introduce a factor of  $(1 - e^{-\beta\omega_p})$  to the scattering width  $\Gamma_C = -2\text{Im}(\Sigma_4)$  [35,36]. The width is most easily analyzed in the center-of-momentum frame. Defining  $\mathbf{K} = (\mathbf{k}_1 + \mathbf{k}_2)/2$  and  $\mathbf{Q} = (\mathbf{k}_1 - \mathbf{k}_2)/2$  and assuming small momenta as in the previous section the width can be approximated roughly as

$$\begin{aligned} \Gamma_C &\approx \frac{\omega_p}{2\pi\beta^2} \int d^2\mathbf{K} d^2\mathbf{Q} \\ &\times \frac{W(\mathbf{p}, \mathbf{K}, \mathbf{Q})}{\omega_{\mathbf{K}+\mathbf{Q}}\omega_{\mathbf{K}-\mathbf{Q}}(2\omega_{\mathbf{K}} + 2\omega_{\mathbf{Q}} - \omega_p - 2\Delta)} \\ &\times \delta(2\omega_0(p^2 + K^2 - Q^2 - 2\mathbf{p} \cdot \mathbf{K})), \end{aligned} \quad (\text{A11})$$

$$\begin{aligned} W(\mathbf{p}, \mathbf{K}, \mathbf{Q}) &= V_{\mathbf{K}+\mathbf{Q}, \mathbf{K}-\mathbf{Q}, \mathbf{p}, 2\mathbf{K}-\mathbf{p}}^{(4)} \\ &\times (2V_{\mathbf{p}, 2\mathbf{K}-\mathbf{p}, \mathbf{K}+\mathbf{Q}, \mathbf{K}-\mathbf{Q}}^{(4)} + V_{\mathbf{p}, 2\mathbf{K}-\mathbf{p}, \mathbf{K}-\mathbf{Q}, \mathbf{K}+\mathbf{Q}}^{(4)}). \end{aligned} \quad (\text{A12})$$

In contrast to the previous section, all states are available for this kind of scattering,  $\Gamma_C > 0$  for all  $\mathbf{p}$ . The  $\delta$  function is

used to eliminate the angular integral for  $\mathbf{K}$ . In terms of the dimensionless variable  $z$  the width can be written

$$\Gamma_C = \left(\frac{\alpha}{8S}\right)^2 \frac{z + \beta\Delta}{4\beta^3\omega_0^4} I(z, \beta\Delta), \quad (\text{A13})$$

where  $I$  is a dimensionless integral given by the rather complicated expression

$$\begin{aligned} I(z, \beta\Delta) &= \int_0^{z_c} dx \int_{(\sqrt{x}-\sqrt{z})^2}^{(\sqrt{x}+\sqrt{z})^2} dy \\ &\times \frac{F(x, y, z, \beta\Delta)}{\sqrt{[(\sqrt{x} + \sqrt{z})^2 - y][y - (\sqrt{x} - \sqrt{z})^2]}} \\ &\times \frac{1}{2(x+y) - z + \beta\Delta}, \\ F &= \frac{1}{a\sqrt{a^2 - b^2}} \left[ V_1 + \frac{a}{b^2} (a - \sqrt{a^2 - b^2}) V_2 \right. \\ &+ \frac{a\sqrt{a^2 - b^2} - a^2 + b^2}{b^2} V_3 \\ &\left. + \frac{(a - \sqrt{a^2 - b^2})^2}{b^2} V_4 \right], \\ a &= x + y + \beta\Delta, \quad b = \sqrt{2xy}, \\ V_1 &= \frac{1}{4}(3x + z - y)x + z - 3y, \\ V_2 &= 3xy - 8\sqrt{xyz} \cos\phi, \\ V_3 &= 4yz, \quad V_4 = 4yz \cos^2\phi, \quad \cos\phi = \frac{x + z - y}{2\sqrt{xz}}. \end{aligned} \quad (\text{A14})$$

A normalized plot of  $I$  vs  $\beta\Delta$  is shown in Fig. 8 for several values of  $z$ . For  $z < 0.5$ , the integral scales as  $1/\beta\Delta < I < 1/\sqrt{\beta\Delta}$ . From this we conclude that the scattering width Eq. (A13) scales weakly with the field at small momenta, where the Bose distribution gives the largest contribution. Changes in the magnon resistivity due to conservative scattering are, therefore, governed primarily by the change in magnon number. Because  $\Gamma_C$  is only weakly suppressed by

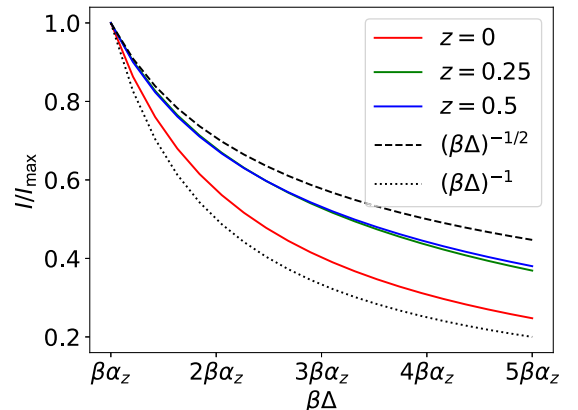


FIG. 8. Scaling of the dimensionless integral  $I$  with parameter  $\beta\Delta$ .

the external field, the magnon resistivity,  $\rho \sim \Gamma/N_0$ , is still enhanced due to the suppression in magnon number. At higher

temperatures  $\Gamma \approx \Gamma_C$ , and so the MMR effect will be much smaller, and governed by changes in magnon number.

- 
- [1] K. Uchida, S. Takahashi, K. Harii, J. Ieda, W. Koshibae, K. Ando, S. Maekawa, and E. Saitoh, Observation of the spin Seebeck effect, *Nature (London)* **455**, 778 (2008).
- [2] C. M. Jaworski, R. C. Myers, E. Johnston-Halperin, and J. P. Heremans, Giant spin Seebeck effect in a non-magnetic material, *Nature (London)* **487**, 210 (2012).
- [3] S. Y. Huang, X. Fan, D. Qu, Y. P. Chen, W. G. Wang, J. Wu, T. Y. Chen, J. Q. Xiao, and C. L. Chien, Transport magnetic proximity effects in platinum, *Phys. Rev. Lett.* **109**, 107204 (2012).
- [4] L. J. Cornelissen, J. Liu, R. A. Duine, J. B. Youssef, and B. J. van Wees, Long-distance transport of magnon spin information in a magnetic insulator at room temperature, *Nat. Phys.* **11**, 1022 (2015).
- [5] X. Y. Wei, O. A. Santos, C. H. S. Lusero, G. E. W. Bauer, J. Ben Youssef, and B. J. van Wees, Giant magnon spin conductivity in ultrathin yttrium iron garnet films, *Nat. Mater.* **21**, 1352 (2022).
- [6] S. S.-L. Zhang and S. Zhang, Magnon mediated electric current drag across a ferromagnetic insulator layer, *Phys. Rev. Lett.* **109**, 096603 (2012).
- [7] J. Li, Y. Xu, M. Aldosary, C. Tang, Z. Lin, S. Zhang, R. Lake, and J. Shi, Observation of magnon-mediated current drag in Pt/yttrium iron garnet/Pt(Ta) trilayers, *Nat. Commun.* **7**, 10858 (2016).
- [8] H. Wu, C. H. Wan, X. Zhang, Z. H. Yuan, Q. T. Zhang, J. Y. Qin, H. X. Wei, X. F. Han, and S. Zhang, Observation of magnon-mediated electric current drag at room temperature, *Phys. Rev. B* **93**, 060403(R) (2016).
- [9] Y. Xie, Y. Yuan, M. Birowska, C. Zhang, L. Cao, M. Wang, J. Grenzer, D. Kriegner, P. Doležal, Y.-J. Zeng, X. Zhang, M. Helm, S. Zhou, and S. Prucnal, Strain-induced switching between noncollinear and collinear spin configuration in magnetic  $Mn_3Ge_3$  films, *Phys. Rev. B* **104**, 064416 (2021).
- [10] D. J. O'Hara, T. Zhu, A. H. Trout, A. S. Ahmed, Y. K. Luo, C. H. Lee, M. R. Brenner, S. Rajan, J. A. Gupta, D. W. McComb, and R. K. Kawakami, Room temperature intrinsic ferromagnetism in epitaxial manganese selenide films in the monolayer limit, *Nano Lett.* **18**, 3125 (2018).
- [11] D. R. Klein, D. MacNeill, J. L. Lado, D. Soriano, E. Navarro-Moratalla, K. Watanabe, T. Taniguchi, S. Manni, P. Canfield, J. Fernández-Rossier, and P. Jarillo-Herrero, Probing magnetism in 2D van der Waals crystalline insulators via electron tunneling, *Science* **360**, 1218 (2018).
- [12] S. Jiang, L. Li, Z. Wang, K. F. Mak, and J. Shan, Controlling magnetism in 2D  $CrI_3$  by electrostatic doping, *Nat. Nanotechnol.* **13**, 549 (2018).
- [13] J.-U. Lee, S. Lee, J. H. Ryoo, S. Kang, T. Y. Kim, P. Kim, C.-H. Park, J.-G. Park, and H. Cheong, Ising-type magnetic ordering in atomically thin  $FePS_3$ , *Nano Lett.* **16**, 7433 (2016).
- [14] B. Huang, M. A. McGuire, A. F. May, D. Xiao, P. Jarillo-Herrero, and X. Xu, Emergent phenomena and proximity effects in two-dimensional magnets and heterostructures, *Nat. Mater.* **19**, 1276 (2020).
- [15] C. Gong and X. Zhang, Two-dimensional magnetic crystals and emergent heterostructure devices, *Science* **363**, eaav4450 (2019).
- [16] T. Song, X. Cai, M. W.-Y. Tu, X. Zhang, B. Huang, N. P. Wilson, K. L. Seyler, L. Zhu, T. Taniguchi, K. Watanabe, M. A. McGuire, D. H. Cobden, D. Xiao, W. Yao, and X. Xu, Giant tunneling magnetoresistance in spin-filter van der Waals heterostructures, *Science* **360**, 1214 (2018).
- [17] Y. Deng, Y. Yu, Y. Song, J. Zhang, N. Z. Wang, Z. Sun, Y. Yi, Y. Z. Wu, S. Wu, J. Zhu, J. Wang, X. H. Chen, and Y. Zhang, Gate-tunable room-temperature ferromagnetism in two-dimensional  $Fe_3GeTe_2$ , *Nature (London)* **563**, 94 (2018).
- [18] J. He, S. Ma, P. Lyu, and P. Nachtigall, Unusual Dirac half-metallicity with intrinsic ferromagnetism in vanadium trihalide monolayers, *J. Mater. Chem. C* **4**, 2518 (2016).
- [19] Q. Sun and N. Kioussis, Prediction of manganese trihalides as two-dimensional Dirac half-metals, *Phys. Rev. B* **97**, 094408 (2018).
- [20] V. V. Kulish and W. Huang, Single-layer metal halides  $MX_2$  ( $X = Cl, Br, I$ ): Stability and tunable magnetism from first principles and Monte Carlo simulations, *J. Mater. Chem. C* **5**, 8734 (2017).
- [21] M. Gibertini, M. Koperski, A. F. Morpurgo, and K. S. Novoselov, Magnetic 2D materials and heterostructures, *Nat. Nanotechnol.* **14**, 408 (2019).
- [22] Y. Yao, X. Zhan, M. G. Sendeku, P. Yu, F. T. Dajan, C. Zhu, N. Li, J. Wang, F. Wang, Z. Wang, and J. He, Recent progress on emergent two-dimensional magnets and heterostructures, *Nanotechnology* **32**, 472001 (2021).
- [23] N. D. Mermin and H. Wagner, Absence of ferromagnetism or antiferromagnetism in one- or two-dimensional isotropic Heisenberg models, *Phys. Rev. Lett.* **17**, 1133 (1966).
- [24] Y. Imry and S.-k. Ma, Random-field instability of the ordered state of continuous symmetry, *Phys. Rev. Lett.* **35**, 1399 (1975).
- [25] M. I. Kaganov and A. V. Chubukov, Interacting magnons, *Sov. Phys. Usp.* **30**, 1015 (1987).
- [26] A. P. Ramirez, Colossal magnetoresistance, *J. Phys.: Condens. Matter* **9**, 8171 (1997).
- [27] S. Jin, T. H. Tiefel, M. McCormack, R. A. Fastnacht, R. Ramesh, and L. H. Chen, Thousandfold change in resistivity in magnetoresistive La-Ca-Mn-O films, *Science* **264**, 413 (1994).
- [28] E. Dagotto, T. Hotta, and A. Moreo, Colossal magnetoresistant materials: The key role of phase separation, *Phys. Rep.* **344**, 1 (2001).
- [29] Y. Tokura and Y. Tomioka, Colossal magnetoresistive manganites, *J. Magn. Magn. Mater.* **200**, 1 (1999).
- [30] A. V. Chubukov, Low-temperature properties of Heisenberg ferromagnets with arbitrary spin in the Holstein-Primakoff formalism, *Sov. Phys. JETP* **62**, 762 (1985).
- [31] G. D. Mahan, Nonzero Temperatures, in *Many-Particle Physics* (Springer US, Boston, MA, 2000), pp. 109–185.
- [32] G. Baym and A. M. Sessler, Perturbation-theory rules for computing the self-energy operator in quantum statistical mechanics, *Phys. Rev.* **131**, 2345 (1963).



- [33] M. E. Zhitomirsky and A. L. Chernyshev, Colloquium: Spontaneous magnon decays, *Rev. Mod. Phys.* **85**, 219 (2013).
- [34] J. Villain, Quantum theory of one- and two-dimensional ferro- and antiferromagnets with an easy magnetization plane. I. Ideal 1-d or 2-d lattices without in-plane anisotropy, *J. Phys. France* **35**, 27 (1974).
- [35] A. B. Harris, Energy width of spin waves in the Heisenberg ferromagnet, *Phys. Rev.* **175**, 674 (1968).
- [36] A. B. Harris, D. Kumar, B. I. Halperin, and P. C. Hohenberg, Dynamics of an antiferromagnet at low temperatures: Spin-wave damping and hydrodynamics, *Phys. Rev. B* **3**, 961 (1971).